Inorg. Chem. **2004**, *43*, 2876–2887

Structural Changes upon Reduction of Dipyrido[2,3-a:3′,2′-c]phenazine Probed by Vibrational Spectroscopy, ab Initio Calculations, and Deuteration Studies

Sarah L. Howell,[†] Benjamin J. Matthewson,[†] Matthew I. J. Polson,[†] Anthony K. Burrell,[‡] and Keith C. Gordon*,[†]

Department of Chemistry, University of Otago, Union Place, Dunedin, New Zealand, and Los Alamos National Laboratory, Los Alamos, New Mexico 87545

Received July 11, 2003

A series of bridging ligands, dipyrido[2,3-a:3′,2′-c]phenazine (ppb), dipyrido[2,3-a:3′,2′-c]-6,7-dichlorophenazine ($ppbCl_2$), and dipyrido[2,3-a:3′,2′-c]-6,7-dimethylphenazine ($ppbMe_2$), and their binuclear copper(I) complexes have been synthesized, and their spectral properties were measured. The single-crystal structure of the complex, $[(PPh_3)_2Cu(\mu\text{-}ppbCl_2)Cu(PPh_3)_2](BF4)_2$ in the monoclinic space group *P*21/*c*, 18.2590(1), 21.1833(3), 23.2960(3) Å with $Z = 4$ is reported. The copper(I) complexes are deeply colored through MLCT transitions in the visible region. The vibrational spectra of the ligands have been modeled using ab initio hybrid density functional theory (DFT) methods (B3LYP/6-31G(d)) and compared to experimental FT-Raman and IR data. The DFT calculations are used to interpret the resonance Raman spectra, and thus the electronic spectra, of the complexes. The preferential enhancement of modes associated with the phenanthroline section of the ligands with blue excitation ($\lambda_{exc} = 457.9$ nm) over phenazine-based modes with redder excitation ($\lambda_{exc} = 514.5$ and 632.8 nm) suggests the 2 MLCT transitions terminated on different unoccupied MOs are present under the visible absorption envelope. The radical anion species of the ligands are prepared by the electrochemical reduction of the binuclear copper(I) complexes; no evidence of dechelation prevalent in other copper(I) complexes is observed. The resonance Raman spectra of the reduced complexes are dramatically different from those of the parent species. Across the series common bands are observed at about 1590 and 1570 cm^{-1} which do not shift with reduction but are altered in intensity. The normal-mode analysis of the radical anion species suggests that these normal modes primarily involve bond length distortions that are unaffected by reduction.

Introduction

Polynuclear metal complexes with bridging polpyridyl ligands have considerable utility as photocatalysts[1] and as multielectron-transfer agents.[2] The active species in many of these cases are metal-to-ligand charge-transfer (MLCT) excited states and redox states, respectively.[3] Vibrational spectroscopy may be an incisive probe of the structural changes attendant on metal complexes that are photoexcited or undergo electron-transfer reactions. A paradigm of such work is the demonstration of a localized MLCT excited state for $[Ru(bpy)_3]^{2+}$ probed by time-resolved resonance Raman (TR^3) spectroscopy, in which the $[Ru^{III}(bpy^{\bullet-})(bpy)_2]^{2+*}$ formulation was established on the basis of observing $bpy^{\bullet-}$ features in the TR^3 spectrum.[4] Although it is relatively easy to identify radical anion species of a ligand in such

* To whom correspondence should be addressed. E-mail: kgordon@alkali.otago.ac.nz.

[†] University of Otago.

[‡] Los Alamos National Laboratory.

(1) (a) Nazeeruddin, M. K.; Kay, A.; Rodicio, I.; Humphrey-Baker, R.; Mueller, E.; Liska, P.; Vlachopoulos, N.; Gratzel, M. *J. Am. Chem. Soc.* **1993**, *115*, 6382. (b) Kalyanasundaram, K.; Gratzel, M. *Coord. Chem. Rev.* **1998**, *177*, 347. (c) Moser, J. E.; Bonnote, P.; Gratzel, M. *Coord. Chem. Rev.* **1998**, *177*, 245. (d) Bignozzi, C. A.; Schoonover, J. R.; Scandola, F. *Prog. Inorg. Chem.* **1997**, *44*, 1.

(2) (a) Scandola, F.; Indelli, M. T.; Chiorboli, C.; Bignozzi, C. A. *Top. Curr. Chem.* **1990**, *158*, 73. (b) Balzani, V.; Campagna, S.; Denti, G.; Juris, A.; Serroni, S.; Venturi, M. *Acc. Chem. Res.* **1998**, *31*, 26. (c) Balzani, V.; Gomez-Lopez, M.; Stoddart, J. F. *Acc. Chem. Res.* **1998**, *31*, 405. (d) Venturi, M.; Serroni, S.; Juris, A.; Campagna, S.; Balzani, V. *Top. Curr. Chem.* **1998**, *197*, 193. (e) Ziessel, R.; Hissler, M.; El-Ghayoury, A.; Harriman, A. *Coord. Chem. Rev.* **1998**, *180*, 1251. (f) Ziessel, R.; Harriman, A. *Coord. Chem. Rev.* **1998**, *171*, 331. (g) Scandola, F.; Argazzi, R.; Bignozzi, C. A.; Chiorboli, C.; Indelli, M. T.; Rampi, M. A. In *Supramolecular Chemistry*; Balzani, V., DeCola, L., Eds.; Kluwer: Dordrecht, The Netherlands, 1992; p 235.

(3) DeArmond, M. K.; Myrick, M. L. *Acc. Chem. Res.* **1989**, *22*, 364.

10.1021/ic030225l CCC: $27.50
Published on Web 04/01/2004

complexes it is comparatively more difficult to provide detailed structural information about the changes in ligand structure upon reduction. The level of insight provided by spectral measurements is critically dependent on the assignment of the vibrational spectrum. This can be challenging for ligands with >30 atoms. Modern computational chemistry provides the possibility of disentangling the rich and complex vibrational spectra that most polypyridyl ligands and their radical anions possess, and may also be used to establish the electronic structure of such complexes. For example, Pulay et al. used density functional theory (DFT), implemented with the hybrid B3LYP functional and a mixed basis set, comprising the standard 6-31G* basis on C, O, and H and Ahlrichs' valence triple-ζ (VTZ) on the metal atoms to examine the structure and vibrational spectra of a series of trivalent metal trisacetylacetonate complexes.[5] In a study of $[M(tap)_3]^{2+}$ (M = Fe, Ru, Os; tap = 1,4,5,8-tetraazaphenanthrene) Zheng et al. used the DFT (B3LYP/LanL2DZ).[6] The electronic properties of the HOMO and LUMO were used to explain the efficacy of these complexes in DNA intercalation and electron transfer from the excited-state complexes to guanine. Similar studies were also carried out on other metal complexes in which electronic properties were the focus of the study.[6] The steric effects on electron delocalization in excited states across the radical anion of a variety of ligands has been studied by utilizing a variety of ab initio methods for sections of the polypyridyl ligands. For example, to model 4,4′-diphenyl-2,2′-bipyridine the electron nature of the reduced 4-phenyl pyridine was examined.[7] It was found that in many cases in which phenyl groups are attached to the polypyridyl ligand, reduction appeared to cause a flattening of the two ring systems and a strengthening of the inter-ring linkage. More recently, the MLCT excited state of $[Re(bpy)(CO)_3(4\text{-Etpy})]^+$ (bpy = 2,2′-bipyridine, 4-Etpy = 4-ethylpyridine) was modeled using DFT (B3LYP), with a modified LANL2 basis set for the effective core potential of the Re(I) center and a 6-31G* basis set for the other atoms. From this study the symmetries and normal vibrational modes for the carbonyl stretches have been established.[8]

We have studied ppb (Figure 1) and some of its analogues for the following reasons. (1) Complexes with dipyrido[2,3-a:3′,2′-c]phenazine (ppb) show very interesting excited-state properties, in particular long-lived MLCT excited states, that are attributed to the rigid structure of the ligand and the small coordinate displacements on going from ppb to $ppb^{\bullet-}$.[9] (2). ppb is a structural isomer of dipyrido[3,2-a:2′,3′-c]phenazine (dppz), the complexes of which are widely studied for their

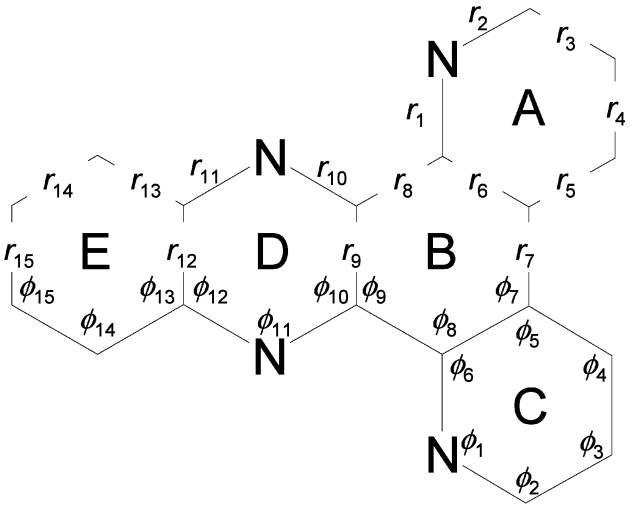

Figure 1. Skeletal structure of ppb with bond parameters and ring labels.

interactions with DNA.[10] The radical anion, $dppz^{\bullet-}$, shows a distinct localization of charge to the phenazine portion of the ligand structure,[11] and it is of interest to see if this localization occurs in the isomer, ppb.

The ligand is advantageous to study, from a computational perspective, because of its C_{2v} symmetry and rigid structure. To further probe the ligand vibrational spectra we have synthesized isotopomers of ppb. The spectra of the radical anion species, $ppb^{\bullet-}$, are collected on the electrochemically reduced complex, $[(PPh_3)_2Cu(\mu\text{-ppb})Cu(PPh_3)_2]^+$and the corresponding $ppbMe_2$ and $ppbCl_2$ complexes.

We restrict our analysis to the 1000−1650 cm^{-1} region of the spectrum because most of the spectroscopic data collected on ppb and its complexes are in that region. A further advantage of this restriction is that we only consider about 20 normal modes of vibration.

Results and Discussion

The ppb ligands are generally only partially soluble in most solvents (ca. 30 mmol L^{-1} in $CHCl_3$). They are emissive under laser radiation in the visible and Raman spectra can only be obtained with NIR excitation.

Crystallographic Data. The crystal structure of $[(PPh_3)_2Cu(\mu\text{-ppb}Cl_2)Cu(PPh_3)_2]^{2+}$ is shown in Figure 2. Crystallographic data are presented in Table 1. While the ligands associated with each of the coppers are bulky, there are no significant difficulties in accommodating the two Cu(I) centers on the same polypyridyl ligand. As with other similar compounds[12] the ppb ligand experiences little apparent

(4) Bradley, P. G.; Kress, N.; Hornberger, B. A.; Dallinger, R. F.; Woodruff, W. H. *J. Am. Chem. Soc.* **1981**, *103*, 7441−7446.
(5) Diaz-Acosta, I.; Baker, J.; Cordes, W.; Pulay, P. *J. Phys. Chem. A* **2001**, *105*, 238.
(6) (a) Zheng, K. C.; Wang, J. P.; Peng, W. L.; Shen, Y.; Yun, F. C. *Inorg. Chim. Acta* **2002**, *328*, 247. (b) Zheng, K. C.; Wang, J. P.; Peng, W. L.; Shen, Y.; Yun, F. C. *J. Chem. Soc., Dalton Trans.* **2002**, 111.
(7) Damrauer, N. H.; Weldon, B. T.; McCusker, J. K. *J. Phys. Chem. A* **1998**, *102*, 3382.
(8) Dattelbaum, D. M.; Omberg, K. M.; Schoonover, J. R.; Martin, R. L.; Meyer, T. J. *Inorg. Chem.* **2002**, *41*, 6071.
(9) Treadway, J. A.; Loeb, B.; Lopez, R.; Anderson, P. A.; Keene, R. F.; Meyer, T. J. *Inorg. Chem.* **1996**, *35*, 2242.
(10) (a) Chen, W.; Turro, C.; Friedman, L. A.; Barton, J. K.; Turro, N. J. *J. Phys. Chem. B* **1997**, *101*, 6995. (b) Friedman, A. E.; Chambron, J.-C.; Sauvage, J.-P.; Turro, N. J.; Barton, J. K. *J. Am. Chem. Soc.* **1990**, *112*, 4960. (c) Hiort, C.; Lincoln, P.; Nordén, B. *J. Am. Chem. Soc.* **1993**, *115*, 3448. (d) Jenkins, Y.; Friedman, A. E.; Turro, N. J.; Barton, J. K. *Biochemistry* **1992**, *31*, 10809. (e)Turro, C.; Bossmann, S. H.; Jenkins, Y.; Barton, J.; Turro, N. J. *J. Am. Chem. Soc.* **1995**, *117*, 9026.
(11) Matthewson, B. J.; Flood, A.; Polson, M. I. J.; Armstrong, C.; Phillips, D. L.; Gordon, K. C. *Bull. Chem. Soc. Jpn.* **2002**, *75*, 933−942.
(12) Gordon, K. C.; Al-Obaidi, A. H. R.; Jayaweera, P. M.; McGarvey, J. J.; Malone, J. F.; Bell, S. E. J. *J. Chem. Soc., Dalton Trans.* **1996**, 1591−1596.

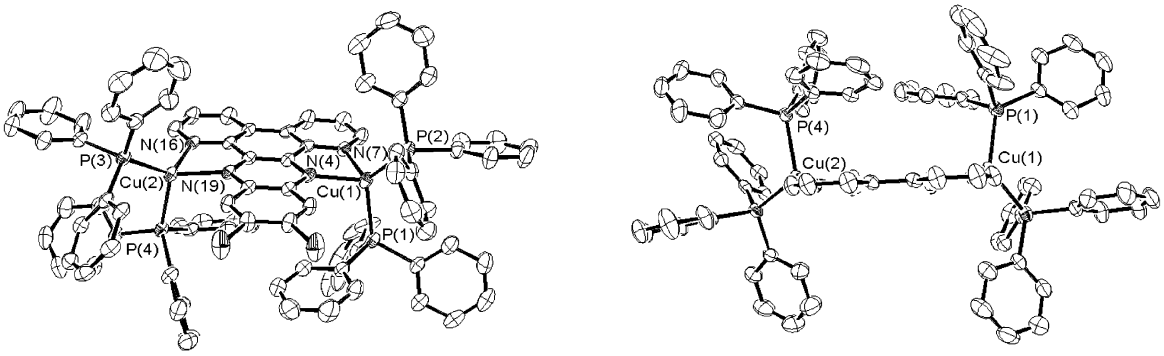

Figure 2. ORTEP drawing of the cation of complex $[(PPh_3)_2Cu(\mu\text{-ppbCl}_2)Cu(PPh_3)_2](BF4)_2{\cdot}4H_2O{\cdot}CH_2Cl_2$. Thermal ellipsoids are drawn at the 50% level. Selected bond lengths (Å) Cu(1)−P(1) 2.2982(12), Cu(1)−P(2) 2.2595(12), Cu(1)−N(4) 2.156(3), Cu(1)−N(7) 2.080(4), Cu(2)−P(3) 2.2599(12), Cu(2)−P(4) 2.3038(12), Cu(2)−N(16) 2.100(3), Cu(2)−N(19) 2.123(3) and angles (°) P(1)−Cu(1)−P(2) 122.81(5), P(1)−Cu(1)−N(4) 105.06(10), P(1)−Cu(1)−N(7) 111.71(10), P(2)−Cu(1)−N4 113.43(10), P(2)−Cu(1)−N(7) 115.81(10), N(4)−Cu(1)−N(7) 78.98(13), P(3)−Cu(2)−P4 113.37(4), P(3)−Cu(2)−N(16) 127.41(10), P(3)−Cu(2)−N(19) 122.69(9), P(4)−Cu(2)−N(16) 101.76(10), P(4)−Cu(2)−N(19) 107.07(9), N(16)−Cu(2)−N(19) 78.66(14).

Table 1. Crystallographic Data for $[(PPh_3)_2Cu(\mu\text{-ppbCl}_2)Cu(PPh_3)_2](BF4)_2{\cdot}4H_2O{\cdot}CH_2Cl_2$

empirical formula	$C_{91}H_{70}B_2Cl_4Cu_2F_8N_4O_4$
temperature /K	203
λ/Å	0.71073
cryst syst	Monoclinic
space group	*P*21/*c* (No. 14)
a/Å	18.2590(1)
b/Å	21.1833(3)
c/Å	23.2960(3)
β/deg	97.226(1)
V/Å^3	8939.0(2)
Z	4
μ(Mo Kα)/mm^{-1}	0.727
D_{calcd}/g cm^{-3}	1.375
no. of observed reflns	15655
no. of uniq reflns	10755
R1, wR2[a]	0.0606, 0.1961

[a] $R1 = \sum F_o - |F_c|/\sum|F_c|$; $wR2 = [\sum[w(F_o^2 - F_c^2)^2]/\sum[w(F_o^2)^2]]^{1/2}$.

distortion. The geometry of the copper atoms is significantly distorted from tetrahedral. This is due to the small "bite" of the polypyridyl ligand. The Cu−N bond lengths are somewhat longer (2.080(4)−2.156(3) Å) than those found in other similar Cu(I) pyridyl complexes (2.018(1)−2.089(7) Å).[13] However, the distortion in the ligand coordination geometry is necessary to allow the ppb ligand to remain effectively flat and yet accommodate the bulky triphenylphosphine ligands. Interestingly, the triphenylphosphine ligands have not adopted a geometry which would place them at the greatest distance from each other, but phosphines P(1) and P(4) assume a geometry which appears to be more congested (Figure 2) than that observed in previous structures.[12]

Neutral Ligand: Calculations and Spectra. The structural parameters of ppb are described using the labeling system depicted in Figure 1.

A selection of calculated bond lengths and angles for ppb are presented in Table 2 along with the corresponding crystallographic data of $[(PPh_3)_2Cu(\mu\text{-ppbCl}_2)Cu(PPh_3)_2]^{2+}$. The calculated structure of ppb (B3LYP/6-31G(d)) predicts short (∼1.35−1.33 Å) bonds for the C−N linkages, r_1, r_2, r_{10}, and r_{11}, with longer C−C bonds (typically ∼1.44−1.40 Å) for the rest of the ligand skeleton. The predicted structure of $ppbCl_2$ compares favorably to the crystal structure of $[(PPh_3)_2Cu(\mu\text{-ppbCl}_2)Cu(PPh_3)_2]^{2+}$ with only r_9 showing a greater than 20 pm difference. This contrasts with the comparison of metal dppz complex crystallographic data and calculations on the dppz ligand.[11] In that case a large number of bonds in the calculated geometry showed differences of greater than 20 pm from crystallographic data. The reason for this is attributed to two factors: (1) The crystal packing forces for the experimental data lead to experimental structural parameters beyond the consideration of the calculations used, which were on a single ligand molecule. (2) The metal moieties (Ru(II) and Re(I)) bound to the dppz ligand in the experimental data are known to interact strongly with the ligand, resulting in further structural distortions not relevant to the calculation of the ligand structure. The good agreement between the calculated geometry of $ppbCl_2$ and the crystal structure of $[(PPh_3)_2Cu(\mu\text{-ppbCl}_2)Cu(PPh_3)_2]^{2+}$ would suggest that the $\{Cu(PPh_3)_2\}^+$ moieties are not structurally demanding on the ligand.[14] The optimized structures of $ppbCl_2$, $ppbMe_2$, and ppb are almost identical with only r_{15} showing significant differences. The substitution effects are structurally localized to the E-ring system.

The optimized structures of ppb and the other ligands were used in calculating vibrational frequencies.[15] The calculated and observed vibrational data in the 1000−1650 cm^{-1} region for ppb, its deuterated analogues, substituted ppb, and complexes thereof are presented in Table 3. The calculated Raman intensities are for 1064 nm excitation and the frequencies presented are scaled by 0.96 following the findings of Radom et al.[16] The calculation produced no imaginary frequencies consistent with an energy minimum for the geometry used.

The experimentally observed and calculated vibrational data are presented in Table 3. The spectra (Figure 3) are

(13) (a) Dobson, J. F.; Green, B. E.; Healy, P. C.; Kennard, C. H. L.; Pakawatchai, C.; White, A. H. *Aust. J. Chem.* **1984**, *37*, 649. (b) Hämäläinen, R.; Ahlgrén, M.; Turpeinen, U.; Raikas, T. *Cryst. Struct. Commun.* **1979**, *8*, 75. (c) Dessy, G.; Fares, V. *Cryst. Struct. Commun.* **1979**, *8*, 507. (d) Burke, P. J.; Henrick, K.; McMillin, D. R. *Inorg. Chem.* **1982**, *21*, 1881. (e) Burke, P. J.; McMillin, D. R.; Robinson, W. R. *Inorg. Chem.* **1980**, *19*, 1211.

(14) Jameson, R. F. In *Metal Ions in Biological Systems*, Vol. 12; Sigul, H., Ed.; Marcel Dekker: New York, 1981; Chapter 1.

(15) A complete listing of all of the calculated vibrational data is given in Table S1 in the Supporting Information.

(16) Scott, A. P.; Radom, L. *J. Phys. Chem.* **1996**, *100*, 16502.

Table 2. Bond Lengths and Angles Calculated Using ab Initio Methods and from the Crystal Structure $[(PPh_3)_2Cu(\mu\text{-}ppbCl_2)Cu(PPh_3)_2]^{2+}$

bond parameters[a]	calculated B3LYP/6-31G(d)			$[(PPh_3)_2Cu(\mu\text{-}ppbCl_2)Cu(PPh_3)_2]^{2+}$	calculated B3LYP/6-31G(d)		
	ppb	$ppbCl_2$	$ppbMe_2$		$ppb^{\bullet-}$	$ppbCl_2^{\bullet-}$	$ppbMe_2^{\bullet-}$
r_1	1.347	1.347	1.348	1.361	1.363	1.361	1.362
r_2	1.326	1.326	1.326	1.342	1.319	1.320	1.320
r_3	1.402	1.403	1.403	1.388	1.408	1.407	1.408
r_4	1.383	1.383	1.383	1.375	1.383	1.383	1.384
r_5	1.408	1.409	1.409	1.413	1.408	1.408	1.407
r_6	1.418	1.417	1.418	1.397	1.433	1.431	1.434
r_7	1.467	1.467	1.467	1.464	1.451	1.453	1.450
r_8	1.472	1.472	1.472	1.460	1.458	1.458	1.458
r_9	1.439	1.441	1.437	1.417	1.435	1.430	1.435
r_{10}	1.327	1.327	1.329	1.343	1.346	1.349	1.347
r_{11}	1.350	1.349	1.348	1.367	1.367	1.361	1.366
r_{12}	1.435	1.431	1.432	1.426	1.437	1.438	1.433
r_{13}	1.423	1.420	1.421	1.414	1.413	1.412	1.411
r_{14}	1.374	1.374	1.376	1.368	1.393	1.393	1.395
r_{15}	1.424	1.433	1.444	1.420	1.404	1.403	1.418
ϕ_1	118	118	118	118	119	119	119
ϕ_2	123	123	123	123	124	124	124
ϕ_3	118	118	118	118	118	118	118
ϕ_4	120	120	120	120	121	120	121
ϕ_5	117	117	117	117	117	117	117
ϕ_6	123	123	123	123	122	122	122
ϕ_7	120	120	120	120	120	120	120
ϕ_8	120	120	120	120	121	121	121
ϕ_9	120	120	120	120	120	120	120
ϕ_{10}	122	122	122	122	122	122	122
ϕ_{11}	117	117	117	117	116	116	116
ϕ_{12}	121	121	121	121	122	122	122
ϕ_{13}	119	119	119	119	119	119	118
ϕ_{14}	120	120	121	121	121	121	121
ϕ_{15}	121	120	120	120	120	120	120

[a] Bond lengths (r)/Å, bond angles (ϕ)/degrees. Labels are given in Figure 1.

rich and complex in the 1000−1650 cm^{-1} region. Generally, the normal modes of vibration associated with the observed vibrational transitions involve nuclei motion of many atoms. The form of the normal mode may be described by the percentage potential energy distribution (%PED) which is parametrized in terms of motions of CH at the A and C rings (A_H), CH at the E ring (E_H), CC at the AB rings (A_C), and CC at the DE rings (DE_C). In the region discussed there are no contributions from out-of-plane modes. The changes in the vibrational modes of ppb and its isotopomers or substituted ppb species are tracked using available programs.[17] These analyses provide a general ring-by-ring description of the normal modes. A selection of normal modes of vibration for ppb and $ppb^{\bullet-}$ are shown in Figure 4.

The IR spectrum of ppb shows 15 bands of moderate to strong intensity in the 1000−1650 cm^{-1} region. At high wavenumber for ppb a band is observed at 1602 cm^{-1}. This is predicted by the calculation to lie at 1610 cm^{-1} and is labeled ν_{79}. For the d_4-ppb (deuteration on the E-ring, Figure 1) a band is observed also at 1602 cm^{-1} which corresponds to a calculated band at 1610 cm^{-1} labeled ν_{80} which has IR intensity. The spectra therefore appear the same in this spectral region. d_{10}-substitution also causes no shift in the observed intense IR bands despite a predicted shift in the ν_{79} to 1586 cm^{-1}. This mode has very little %PED from the D and E ring systems and is mainly an ABC ring mode.

(17) (a) Grafton, A. K.; Wheeler, R. A. *Comput. Phys. Commun.* **1998**, *113*, 78. (b) Grafton, A. K.; Wheeler, R. A. *J. Comput. Chem.* **1998**, *19*, 1663.

ν_{74}, observed at 1540 cm^{-1} for ppb and predicted at 1548 cm^{-1}, shifts with both d_4- and d_{10}-substitution. For d_{10}-ppb a strong band is observed at 1510 cm^{-1} (predicted at 1515 cm^{-1}); for d_4-ppb a weaker feature appears at 1532 cm^{-1}. This band is predicted at 1536 cm^{-1} and the diminished relative intensity is also predicted. The ν_{74} mode is predominantly an ABC mode with 70%PED contributions from these 3 rings.

The IR spectral region from 1400 to 1500 cm^{-1} is complex and interesting. For ppb a number of strong IR absorptions are observed: lying at 1494, 1485, and 1428 cm^{-1}. These correspond to ν_{73}, ν_{72}, and ν_{69}, respectively. d_4-substitution results in increased intensities for other modes in this region. Experimentally bands are observed at 1489, 1471, 1428, and 1412 cm^{-1}. Calculations predict this band pattern with ν_{73}, ν_{70}, ν_{71}, and ν_{67}, all having comparable relative intensities. d_{10}-substitution results in diminished band intensity in this region, with ν_{72} observed at 1442 cm^{-1} and predicted at 1448 cm^{-1} being the only strong feature. ν_{73}, which appears for each of the isotopomers, is a delocalized normal mode.

The spectral region 1400−1180 cm^{-1} is relatively uncongested; two strong bands are observed in the IR spectrum of ppb, within this region. These lie at 1367 and 1203 cm^{-1}; they are predicted at 1360 (ν_{66}) and 1207 cm^{-1} (ν_{57}). d_4-deuteration is predicted to give rise to a greater number of IR transitions in this region; strong bands are observed at 1360, 1275, and 1194 cm^{-1} corresponding to predicted bands at 1357 (ν_{66}), 1287 (ν_{60}), and 1209 cm^{-1} (ν_{57}). d_{10}-ppb also shows a number of bands in this region. These are observed at 1321, 1261, 1253, 1209, and 1178 cm^{-1} and correspond

Table 3. Calculated and Experimental Wavenumbers and Intensities for Ppb, Its Isotopomers, $PpbMe_2$, and $PpbCl_2$

		ppb ν/cm^{-1} (Int.)[c]		d_4-ppb ν/cm^{-1} (Int.)		d_{10}-ppb ν/cm^{-1} (Int.)		$ppbCl_2$ ν/cm^{-1} (Int.)			$ppbMe_2$ ν/cm^{-1} (Int.)	
%PED[a]	mode[b]	calc.	exp.	calc.	exp.	calc.	exp.	calc.	exp.	mode[d]	calc.	exp.
E_H (40), DE_C (55)	48 a_1	1007 (4, 5)	1011 (0, 9)					1096 (82, 5)	1106 (47, 5)			
A_H (20), A_C (65), DE_C (10)	49 a_1	1055 (18, 14)	1055 (14, 19)	1054 (15, 16)	1055 (11, 22)	1059 (46, 13)	1061 (28, 15)	1055 (4, 10)	1054 (0, 21)	53	1005 (48, 1)	1000 (21, 0)
A_H (35), A_C (55), DE_C (5)	50 b_2	1072 (18, 0)	1071 (16, 0)	1074 (26, 0)	1074 (21, 0)			1072 (5, 0)	1071 (8, 0)	54	1024 (0, 0)	
A_H (20), A_C (40), DE_C (20)	51 a_1	1086 (55, 0)	1099 (43, 2)	1084 (43, 0)	1093 (36, 0)			1083 (2, 3)	1095 (0, 2)	55	1039 (11, 0)	1021 (10, 0)
A_H (15), E_H (20), A_C (30), DE_C (35)	52 a_1	1126 (42, 1)	1121 (25, 3)	1131 (22, 0)	1124 (17, 0)			1135 (46, 0)	1128 (64, 0)	56	1055 (12, 13)	1054 (2, 22)
E_H (50), A_C (0), DE_C (40)	53 b_2	1132 (12, 0)	1137 (13, 0)					1258 (0, 0)		57	1057 (0, 0)	
A_H (60), A_C (30), DE_C (5)	54 b_2	1135 (5, 2)	1143 (0, 3)	1135 (2, 2)	1145 (0, 1)			1136 (0, 2)	1129 (0, 2)	58	1072 (13, 0)	1071 (13, 0)
E_H (55), A_C (15), DE_C (15)	55 a_1	1159 (0, 0)								59	1087 (39, 1)	1095 (26, 0)
A_H (25), A_C (10), DE_C (50)	56 b_2	1207 (13, 0)	1212 (0, 6)	1212 (19, 0)	1212 (19, 2)	1210 (36, 3)	1209 (27, 4)	1201 (6, 1)	1197 (30, 3)	60	1115 (0, 0)	
A_H (50), A_C (30), DE_C (15)	57 a_1	1213 (36, 4)	1203 (34, 0)	1209 (16, 3)	1194 (37, 0)	975 (0, 1)	985 (12, 0)	1210 (23, 2)	1209 (15, 6)	61	1133 (24, 1)	1127 (20, 0)
E_H (45), A_C (10), DE_C (45)	58 b_2	1237 (2, 0)		1258 (1, 0)		1034 (6, 1)	1042 (11, 0)	1229 (3, 0)	1226 (3, 0)	62	1138 (1, 2)	
E_H (10), A_C (20), DE_C (65)	59 a_1	1244 (2, 10)		1244 (1, 11)		1250 (51, 9)	1253 (35, 0)	1227 (0, 6)		63	1190 (8, 7)	1190 (0, 7)
A_H (10), A_C (45), DE_C (40)	60 a_1	1268 (16, 6)	1258 (10, 6)	1287 (81, 5)	1275 (59, 4)	1188 (13, 13)	1178 (45, 0)	1263 (20, 11)	1256 (15, 7)	64	1211 (10, 0)	1207 (36, 7)
A_C (80), DE_C (10)	61 b_2	1288 (3, 3)	1278 (0, 6)	1293 (1, 1)	1292 (0, 4)	1294 (1, 8)		1294 (1, 1)	1287 (0, 4)	65	1213 (39, 3)	
A_H (30), A_C (30), DE_C (40)	62 b_2	1306 (0, 6)	1306 (0, 4)	1312 (0, 10)	1308 (0, 4)	1002 (0, 0)		1313 (1, 8)	1308 (0, 7)	66	1237 (0, 8)	
A_H (25), A_C (70), DE_C (5)	63 a_1	1322 (2, 25)	1336 (0, 28)	1323 (0, 28)	1335 (0, 28)	1266 (89, 1)	1261 (70, 6)	1322 (0, 17)	1326 (0, 21)	67	1245 (2, 0)	1239 (4, 0)
E_H (20), A_C (20), DE_C (60)	64 a_1	1349 (19, 17)	1342 (17, 0)			1306 (0, 5)		1347 (1, 15)	1340 (0, 20)	68	1268 (22, 11)	1257 (15, 10)
E_H (40), A_C (10), DE_C (45)	65 b_2	1353 (7, 4)								69	1272 (0, 1)	
A_H (10), A_C (5), DE_C (80)	66 a_1	1360 (77, 7)	1367 (96, 5)	1357 (46, 17)	1360 (100, 3)	1364 (2, 88)	1394 (0, 100)	1359 (26, 10)	1360 (61, 4)	70	1296 (2, 1)	1307 (5, 11)
A_H (15), A_C (40), DE_C (45)	67 a_1	1398 (99, 100)	1388 (0, 10)	1397 (100, 100)	1412 (49, 100)			1396 (19, 100)	1401 (0, 59)	71	1317 (0, 13)	
A_H (15), A_C (5), DE_C (80)	68 a_1	1409 (9, 48)	1418 (0, 100)	1401 (1, 61)	1392 (9, 52)	1393 (32, 100)	1400 (20, sh)[e]	1409 (1, 38)	1411 (0, 100)	72	1322 (0, 28)	1325 (12, 32)
A_H (50), E_H (10), A_C (30),	69 b_2	1433 (100, 0)	1428 (68, 0)	1417 (57, 1)		1327 (67, 0)	1321 (43, 0)	1419 (8, 0)	1412 (22, 0)	73	1357 (16, 35)	1347 (16, 30)
A_H (45), A_C (35), DE_C (20)	70 b_2	1464 (0, 1)	1463 (0, 6)	1470 (38, 6)	1471 (51, 6)	1397 (0, 2)				74	1362 (67, 12)	1364 (100, 0)
E_H (25), A_C (25), DE_C (30)	71 a_1	1478 (1, 8)	1476 (0, 8)	1436 (69, 2)	1428 (36, 0)	1419 (8, 28)	1419 (12, 0)	1449 (100, 20)	1441 (100, 34)	75	1397 (93, 100)	1413 (40, 100)
E_H (15), A_C (10), DE_C (65)	72 b_2	1488 (49, 4)	1485 (39, 5)			1448 (19, 6)	1442 (43, 16)	1471 (15, 5)	1471 (29, 6)	76	1405 (4, 2)	1406 (28, 0)
A_H (20), E_H (20), A_C (25), DE_C (35)	73 a_1	1502 (66, 0)	1494 (48, 0)	1491 (55, 2)	1489 (41, 1)	1450 (41, 8)	1461 (20, 0)	1488 (16, 1)	1485 (21, 3)	77	1416 (5, 12)	
A_H (20), A_C (50), DE_C (20)	74 a_1	1548 (57, 5)	1540 (45, 27)	1536 (23, 4)	1532 (20, 19)	1515 (100, 6)	1510 (74, 18)	1536 (2, 5)		78	1423 (0, 47)	1452 (0, 41)
DE_C (100)	75 b_2	1548 (3, 16)	1543 (0, 21)	1547 (4, 16)	1541 (0, 15)	1542 (9, 16)	1527 (12, 17)	1548 (1, 21)	1539 (0, 32)	79	1424 (63, 0)	1450 (26, 0)
A_C (25), DE_C (60)	76 a_1	1567 (1, 4)	1570 (0, 8)	1559 (22, 6)	1561 (15, 7)	1546 (8, 1)	1543 (13, 0)	1559 (8, 3)		80	1458 (4, 0)	
A_H (20), A_C (76),	77 b_2	1581 (3, 7)	1584 (0, 26)	1579 (4, 7)	1573 (0, 20)	1560 (0, 13)		1580 (0, 7)	1577 (0, 23)	81	1468 (0, 2)	
A_H (25), A_C (70)	78 a_1	1606 (7, 27)	1597 (0, 41)	1606 (7, 27)	1597 (0, 40)	1577 (11, 39)	1566 (21, 38)	1606 (1, 23)	1594 (0, 42)	82	1468 (2, 4)	
A_H (20), A_C (70),	79 b_2	1610 (38, 2)	1602 (100, 0)	1599 (0, 0)		1586 (41, 1)	1602 (100, 0)	1610 (15, 2)	1594 (12, 0)	83	1469 (100, 39)	1473 (56, 34)
E_H (20), DE_C (80)	80 b_2	1632 (5, 1)	1618 (0, 4)	1610 (43, 2)	1602 (75, 0)	1598 (0, 0)		1604 (5, 0)		84	1485 (26, 2)	
										85	1485 (0, 14)	
										86	1490 (58, 5)	1481 (58, 0)
										87	1500 (37, 1)	1488 (58, 0)
										88	1542 (15, 5)	1535 (19, 0)
										89	1544 (4, 24)	1535 (0, 47)
										90	1563 (13, 4)	1562 (7, 8)
										91	1581 (1, 8)	1582 (0, 36)
										92	1606 (8, 31)	1593 (0, 58)
										93	1610 (27, 3)	1589 (18, 0)
										94	1643 (11, 2)	

[a] Potential energy distribution of normal mode of vibration, see text for details. [b] Mode number and symmetry for ppb. [c] Relative intensities for bands IR and Raman, respectively, normalized such that the most intense band in the reported spectral region is 100. [d] Mode number for $PpbMe_2$. [e] The experimental data has a broad band at 1394 cm^{-1} with a faint shoulder at 1400 cm^{-1}. This band encompasses predicted modes 66 and 68.

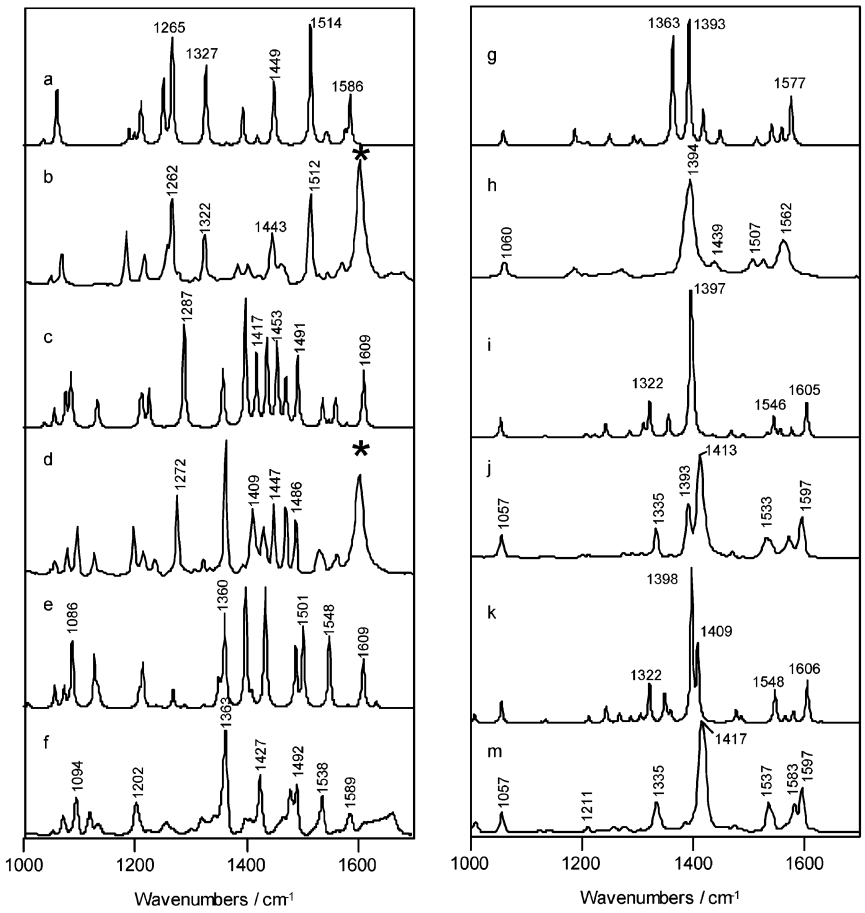

Figure 3. Trace a: Calculated IR spectrum of d_{10}-ppb. Trace b: IR spectrum of d_{10}-ppb in KBr disk (*water band). Trace c: Calculated IR spectrum of d_4-ppb. Trace d: IR spectrum of d_4-ppb in $CDCl_3$ solution (solvent subtracted, *water band). Trace e: Calculated IR spectrum of ppb. Trace f: IR spectrum of ppb in $CDCl_3$ solution (solvent subtracted). Trace g: Calculated Raman spectrum of d_{10}-ppb. Trace h: FT-Raman spectrum of d_{10}-ppb (solid). Trace i: Calculated Raman spectrum of d_4-ppb. Trace j: FT-Raman spectrum of d_4-ppb (solid). Trace k: Calculated Raman spectrum of ppb. Trace m: FT-Raman spectrum of ppb (solid).

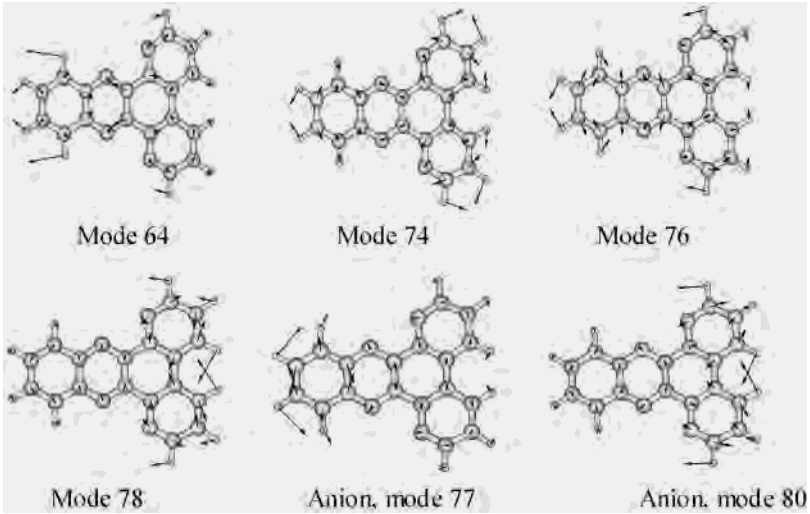

Figure 4. Selected normal modes calculated for ppb and ppb$^{\bullet-}$.

to predicted bands at 1327 (ν_{69}), 1266 (ν_{63}), 1250 (ν_{59}), 1210 (ν_{56}), and 1188 cm^{-1} (ν_{60}).

The spectral region 1180−1000 cm^{-1} shows 5 IR bands for ppb, corresponding to predicted bands for ν_{53} to ν_{49}. d_4-ppb shows fewer bands and d_{10}-ppb shows just three bands at 1061 cm^{-1} (ν_{49}), 1042 cm^{-1} (ν_{58}), and 1178 cm^{-1} (ν_{60}).

The most striking difference between the IR spectrum of ppb and that of $ppbCl_2$ is that the latter has a strong absorption at 1441 cm^{-1} (predicted at 1449 cm^{-1}, ν_{71}) with some weaker bands at 1360, 1128, and 1106 cm^{-1} (predicted at 1359, ν_{66}, 1135, ν_{52}, and 1096, ν_{48}). $ppbMe_2$ possesses more modes than the other systems studied. The IR spectrum

Table 4. Electrochemical Potentials (V)[a] for Ligands[b] and Complexes[c], and Electronic Absorption Band Frequencies (nm) and Extinction Coefficients ($dm^3\ mol^{-1}\ cm^{-1}$) for Ligands[d] and Complexes[e,f]

compound	$E^{\circ\prime}$/V	λ/nm ($\epsilon \times 10^{-3}$/$dm^3\ mol^{-1}\ cm^{-1}$)					
$ppbCl_2$	−1.05	310[s](15)	369 (7)	377 (7)			
ppb	−1.27	307 (26)	365 (14)	374 (13)			
$ppbMe_2$	−1.31	312[s](14)	365 (9)	373 (9)			
$[(PPh_3)_2Cu(\mu\text{-}ppbCl_2)Cu(PPh_3)_2]^{2+}$	−0.38	310[s](21)	383 (13)	415[s](9.4)		603 (6.1)	
$[(PPh_3)_2Cu(\mu\text{-}ppb)Cu(PPh_3)_2]^{2+}$	−0.42	308[s](18)	367 (15)	400[s](8.2)		568 (8.5)	
$[(PPh_3)_2Cu(\mu\text{-}ppbMe_2)Cu(PPh_3)_2]^{2+}$	−0.51	310[s](34)	374 (21)	404[s](14)		552 (11)	
$[(PPh_3)_2Cu(\mu\text{-}ppbCl_2)Cu(PPh_3)_2]^{+}$			355 (16)		497 (6.6)		973 (1.1)
$[(PPh_3)_2Cu(\mu\text{-}ppb)Cu(PPh_3)_2]^{+}$			356 (20)		512 (9.6)	557[s](5.6)	999 (1.8)
$[(PPh_3)_2Cu(\mu\text{-}ppbMe_2)Cu(PPh_3)_2]^{+}$			358 (28)		517 (12)		1034 (2)

[a] $E^{\circ\prime}$ tabulated was the mean voltage of the reduction and oxidation waves. All waves fully reversible. 1 mM dichloromethane solutions. Scan rate of 0.1 V/s. Room temperature (25 °C). [b] Referenced to silver/silver chloride couple (0.22 V). 0.1 M TBAH supporting electrolyte. [c] Referenced to ferrocene/ferrocenium couple (0.4 V). 0.1 M TBAP supporting electrolyte. [d] Dichloromethane solutions. Room temperature (25 °C). [e] 10−50 μM dichloromethane solutions. Room temperature (25 °C). [f] 300−610 nm region. [s] Shoulder feature.

of $ppbMe_2$ is similar to that of ppb, with the strongest feature at 1364 cm^{-1} and bands at 1589, 1535, 1488, 1481, 1473, 1450, 1406, 1413, 1257, and 1207 cm^{-1}. These bands correspond to the $ppbMe_2$ modes 74, 93, 88, 87, 86, 83, 79, 76, 75, 68, and 64, respectively.

The FT-Raman spectrum of ppb shows 6 bands of strong to medium relative intensity in the 1000−1650 cm^{-1} region. In the spectral region 1650−1530 cm^{-1} a number of bands are observed. The band observed at 1597 cm^{-1} corresponds to mode 78, predicted at 1606 cm^{-1} and is an ABC ring mode (Figure 4). The 1584 cm^{-1} band corresponds to mode 77 and is an ABC-ring mode. The band at 1540 cm^{-1} corresponds to mode 74 which involves motion of the ABC and E rings of the ligand. Deuteration to d_4-ppb does not greatly perturb this spectral region. This behavior is predicted by the calculation. These modes are observed to shift in the spectrum of d_{10}-ppb. ν_{78} shifts to 1566 cm^{-1} (predicted at 1577 cm^{-1}) for d_{10}-ppb. Modes 74 and 75 are observed at 1540 and 1543 cm^{-1} for ppb and at 1510 and 1527 cm^{-1} for d_{10}-ppb, respectively; these are predicted at 1515 and 1542 cm^{-1} for d_{10}-ppb.

In the 1300−1450 cm^{-1} region the strongest Raman band is observed; for ppb this lies, as a broad band, at 1418 cm^{-1}. This is consistent with the calculated spectrum having ν_{67} and ν_{68} at 1398 and 1409 cm^{-1} respectively. Mode 67 is a delocalized mode and 68 is a DE ring mode. Upon deuteration to d_4-ppb two strong bands are observed at 1392 and 1412 cm^{-1}. Bands are predicted at 1401 and 1397 cm^{-1}. These bands are shifted to lower frequency in d_{10}-ppb, which has a broad band at 1394 cm^{-1} attributed to predicted bands at 1364 and 1393 cm^{-1}. A band observed at 1336 cm^{-1} in the spectrum of ppb is assigned as mode 63 and is an ABC-ring mode.

The FT-Raman spectrum of $ppbCl_2$ and that of $ppbMe_2$ are similar to ppb. The strongest band lies at 1411 and 1413 cm^{-1} for each of the substituted ppbs − this mode corresponds to mode 68 in ppb and is described as a DE-ring mode. At higher frequencies bands are present in both substituted compounds at 1594/3 cm^{-1} and 1539/5 cm^{-1} that correspond to ppb modes 78 and 75, and $ppbMe_2$ modes 92 and 89. Spectral differences do occur at about 1490 cm^{-1} where $ppbMe_2$ has bands at 1473 and 1452 cm^{-1} that are predicted at 1469 and 1423 cm^{-1}.

The correspondence between the observed and calculated spectra for ppb, its isotopomers, and substituted analogues is sufficient to analyze the resonance Raman spectra of the complexes in terms of the population of π^* MOs on the ppb ligand.

The electronic absorption spectra of the ligands are presented in Table 4. A number of ligand-centered (LC) $\pi \rightarrow \pi^*$ transitions are present. It is possible to model the electronic transitions of the ligand using time-dependent density functional theory (TDDFT).[18] Such calculations (at B3LYP/6-31G(d) level) predict two transitions of reasonable intensity at approximately 400 and 340 nm for each of the ligands.[19] The lowest energy transition is unshifted by substitution as observed in the experimental data. The three lowest energy MOs with their symmetry labels are shown in Figure 5. Each of these are potential acceptor MOs for the metal complex MLCT transitions.

Complexes: Electronic and Resonance Raman Spectra. The binuclear copper(I) complexes with ppb and its substituted analogues are highly colored materials. The electronic absorption spectra in CH_2Cl_2 (Table 4) show that in addition to the ligand-centered transitions above 420 nm each complex has a strong MLCT absorption in the visible region. The MLCT band varies from 600 nm for $[(PPh_3)_2Cu(\mu\text{-}ppbCl_2)Cu(PPh_3)_2]^{2+}$ to 550 nm for $[(PPh_3)_2Cu(\mu\text{-}ppbMe_2)Cu(PPh_3)_2]^{2+}$ and shows solvatochromic behavior. The MLCT transitions correlate with the ease of reduction for the 3 complexes; with $[(PPh_3)_2Cu(\mu\text{-}ppbCl_2)Cu(PPh_3)_2]^{2+}$ being about 130 mV easier to reduce than $[(PPh_3)_2Cu(\mu\text{-}ppbMe_2)Cu(PPh_3)_2]^{2+}$.[20,21]

Resonance Raman spectroscopy can provide some insight into the nature of the resonant spectroscopic transition

(18) Baerends, E. J.; Riccardi, G.; Rosa, A.; van Gisbergen, S. J. A. *Coord. Chem. Rev.* **2002**, *230*, 5.

(19) For ppb the transitions lie at: 401 nm, HOMO-1 → LUMO, f = 0.0014; 333 nm, a combination of HOMO − 2 → LUMO and HOMO → LUMO + 1, f = 0.088. For $ppbCl_2$ the transitions lie at: 401 nm, a combination of HOMO − 5 → LUMO and HOMO − 2 → LUMO, f = 0.0013; 360 nm, a combination of HOMO − 1 → LUMO + 1 and HOMO → LUMO, f = 0.088. For $ppbMe_2$ the transitions lie at: 400 nm, HOMO − 2 → LUMO, f = 0.0014; 360 nm, a combination of HOMO − 1 → LUMO + 1 and HOMO → LUMO, f = 0.0075 and 342 nm, a combination of HOMO −1 → LUMO and HOMO → LUMO + 1, f = 0.12.

(20) (a) Sherborne, J.; Scott, S. M.; Gordon, K. C. *Inorg. Chim. Acta* **1997**, *260*, 199. (b) Sherborne, J.; Gordon, K. C. *Asian J. Spectrosc.* **1998**, *2*, 137.

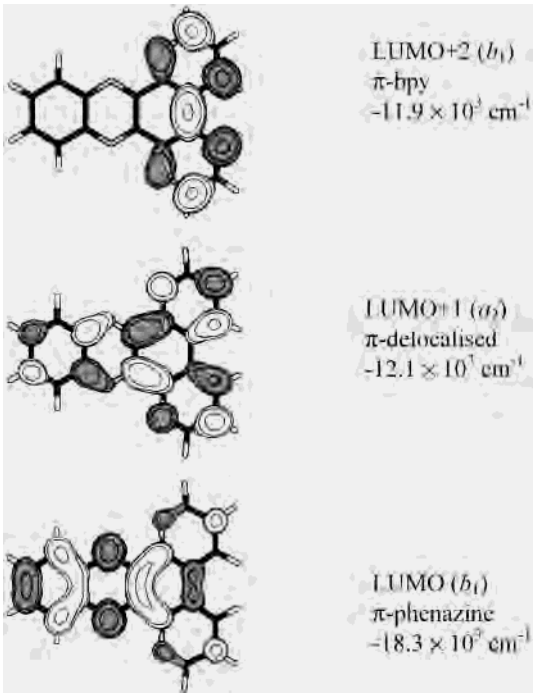

Figure 5. Molecular orbital depictions of ppb showing the MO energy (cm^{-1}) and symmetry.

through the pattern of band intensity enhancements.[22,23] Normal modes that distort the molecule in a fashion similar to the resonant electronic transition show greatest resonance enhancement.[24]

The resonance Raman spectra of the complexes show distinct enhancement patterns on going from 457.9 to 632.8 nm excitation. The resonance Raman spectra of $[(PPh_3)_2Cu(\mu\text{-ppb})Cu(PPh_3)_2]^{2+}$ show enhancement of a large number of modes in the 1000−1650 cm^{-1} region (Figure 6). An analysis of the relative intensities of these spectra reveals that mode 74 (1524 cm^{-1}) is preferentially enhanced with short wavelength excitation (457.9 nm) with modes 76 (1575 cm^{-1}) and 64 (1342 cm^{-1}) showing increased relative enhancement with 514.5-nm excitation.

Analysis of these modes reveals that the red-enhanced modes (76 and 64) are DE-ring modes (see Figure 4), whereas the blue-enhanced mode (ν_{74}) is an ABC-mode. This would support the assignment of the electronic absorption spectra of $[(PPh_3)_2Cu(\mu\text{-ppb})Cu(PPh_3)_2]^{2+}$ as being due to population of a π^* MO based on the phenazine portion of the ligand at redder wavelengths, with a second higher energy transition, populating a π^* MO based on the phenanthroline portion of the ligand. The MO energies suggest that the lowest energy π^* MO (LUMO) is in fact phenazine based (Figure 5). The next highest MOs, both lying about 6000 cm^{-1} higher in energy, are phenazine- (LUMO + 1) and phenathroline-based (LUMO + 2). The resonance Raman data are consistent with an acceptor MO at higher energy that is ABC ring in nature. This suggests that the Cu(I) → LUMO + 2 is absorbing strongly at 457.9 nm.

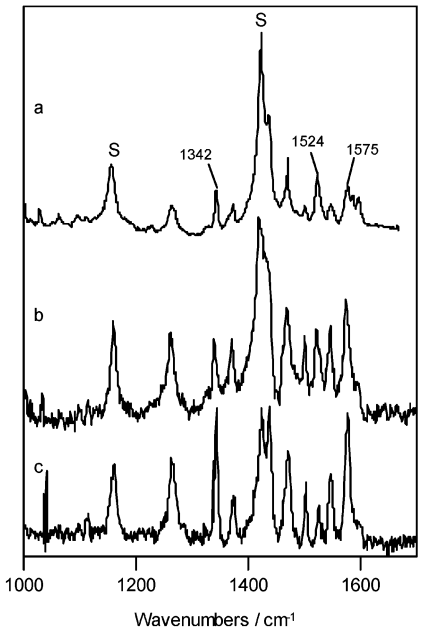

Figure 6. Resonance Raman spectra of $[(PPh_3)_2Cu(\mu\text{-ppb})Cu(PPh_3)_2]^{2+}$ (3 mM CH_2Cl_2 solution) at: λ_{exc} = 457.9 nm (trace a); λ_{exc} = 488 nm (trace b); and λ_{exc} = 514.5 nm (trace c).

Radical Anion: Spectra and Calculations. The structures calculated for ppb and $ppb^{\bullet-}$ are similar. Bonds r_1, r_6, r_{10}, r_{11}, and r_{14} show bond lengthening (Δr > 10 pm) with r_7 and r_{15} shortening (Δr < −10 pm). It is interesting to compare these changes to those calculated for the isomer dppz. The radical anion of dppz shows similar structural changes.[11] The most notable differences being that r_1 is unperturbed by reduction in dppz, and the central phenazine ring (r_9, r_{10}, r_{11}) shows greater structural changes than for ppb/$ppb^{\bullet-}$. Similar changes are observed on going from neutral ligand to radical anion for the calculated structures of $ppbCl_2$ and $ppbMe_2$ (Table 2).

The optimized structures of the radical anions of ppb, $ppbCl_2$, and $ppbMe_2$ were used in calculating vibrational frequencies.[25] The calculated vibrational data in the 1000−1650 cm^{-1} region are presented in Table 5. The calculations produced no imaginary frequencies consistent with an energy minimum for each of the geometries used. The singly occupied MO for each of the calculated radical anion species is the LUMO π^* MO of the corresponding neutral species (Figure 5).

Attempts to generate the UV/visible spectra of $ppb^{\bullet-}$ directly were unsuccessful because the ligand rapidly chelates to the working electrode to form what appears to be a Pt

(21) Lever, A. B. P.; Dodsworth, E. S. In *Inorganic Electronic Structure and Spectroscopy, Volume II, Applications and Case Studies;* Solomon, E. I., Lever, A. B. P., Eds.; J. Wiley and Sons Inc.: New York, 1999; Chapter 4.
(22) Clarke, R. J. H.; Dines, T. J. *Angew. Chem., Int. Ed. Engl.* **1986**, *25*, 131.
(23) (a) Clark, R. J. H.; Turtle, P. C.; Strommen, D. P.; Streusand, B.; Kincaid, J. R.; Nakamoto, K. *Inorg. Chem.* **1977**, *16*, 84. (b) Ma'nuel, D. J.; Strommen, D. P.; Bhuiyan, A.; Sykora, M.; Kincaid, J. R. *J. Raman Spectrosc.* **1997**, *28*, 933. (c) Flood, A.; Girling, R. B.; Gordon, K. C.; Hester, R. E.; Moore, J. N.; Polson, M. I. J. *J. Raman Spectrosc.* **2002**, *32*, 434.
(24) Tsuboi, M.; Hirakawa, A. Y. *Science* **1975**, *188*, 359.

(25) A complete listing of the vibrational data for the radical anion species is given in Table S2 in Supporting Information.

Table 5. Calculated Wavenumbers and Intensities for $ppb^{\bullet-}$, $PpbMe_2^{\bullet-}$, and $PpbCl_2^{\bullet-}$, and Resonance Raman Data for the Electrochemically Reduced Complexes $[(PPh_3)_2Cu(\mu\text{-}ppbX_2)Cu(PPh_3)_2]^+$

			ν/cm^{-1} (Int.)[c]						ν/cm^{-1} (Int.)[c]	
			$ppb^{\bullet-}$		$ppbCl_2^{\bullet-}$				$ppbMe_2^{\bullet-}$	
%PED[a]	mode[b]		calc.	exp.	calc.	exp.	mode[d]		calc.	exp.
E_H (50), DE_C (45)	48	a_1	1022 (1, 4)	1027	1095 (23, 4)		53	a_1	1000 (6, 2)	
A_H (20), A_C (70), DE_C (5)	49	a_1	1041 (4, 16)	1059	1044 (5, 21)		54	b_2	1010 (0, 0)	
A_H (40), A_C (55), DE_C (5)	50	b_2	1055 (0, 12)		1059 (0, 11)		55	a_1	1029 (1, 0)	
A_H (10), A_C (40), DE_C (30)	51	a_1	1075 (0, 3)		1073 (1, 1)		56	a_1	1041 (5, 14)	
E_H (50), DE_C (50)	52	b_2	1105 (0, 1)				57	b_2	1051 (0, 0)	
A_H (20), A_C (45), DE_C (25)	53	a_1	1121 (0, 3)		1127 (2, 4)		58	b_2	1056 (0, 10)	
A_H (65), A_C (30), DE_C (5)	54	b_2	1123 (0, 0)		1124 (0, 1)		59	a_1	1076 (0, 2)	
E_H (80), DE_C (10)	55	a_1	1144 (0, 2)	1149			60	b_2	1092 (2, 5)	
A_H (5), A_C (25), DE_C (70)	56	b_2	1170 (69, 100)		1179 (39, 45)		61	a_1	1121 (0, 3)	
A_H (35), A_C (35), DE_C (15)	57	a_1	1192 (1, 26)	1197	1198 (0, 13)	1214	62	a_1	1126 (0, 0)	
A_H (20), A_C (5), DE_C (70)	58	b_2	1192 (14, 34)		1178 (28, 100)		63	b_2	1168 (79, 100)	
A_H (15), A_C (65), DE_C (15)	59	a_1	1242 (8, 8)		1240 (9, 2)	1257	64	a_1	1187 (3, 3)	
E_H (45), A_C (5), DE_C (45)	60	b_2	1249 (15, 30)		1258 (13, 34)		65	a_1	1192 (0, 23)	
A_C (10), DE_C (80)	61	a_1	1277 (6, 60)	1266	1283 (10, 64)		66	b_2	1199 (7, 18)	
A_H (20), A_C (20), DE_C (50)	62	b_2	1288 (8, 14)		1295 (28, 32)		67	a_1	1245 (5, 3)	
A_H (5), E_H (5), A_C (60), DE_C (30)	63	b_2	1305 (20, 5)		1322 (11, 5)		68	b_2	1254 (12, 25)	
A_C (30), DE_C (60)	64	a_1	1311 (100, 15)	1310	1308 (100, 37)	1298	69	b_2	1261 (0, 0)	
A_C (10), DE_C (80)	65	a_1	1330 (18, 5)	1341	1329 (89, 15)	1335	70	a_1	1295 (11, 60)	
A_H (20), A_C (45), DE_C (30)	66	a_1	1347 (25, 0)		1344 (65, 5)		71	b_2	1297 (19, 10)	
A_H (10), E_H (15), A_C (40), DE_C (30)	67	b_2	1348 (3, 2)				72	a_1	1308 (100, 19)	
A_H (25), A_C (15), DE_C (60)	68	a_1	1376 (0, 4)		1378 (0, 5)		73	a_1	1329 (35, 4)	1328
A_H (20), A_C (40), DE_C (30)	69	a_1	1395 (4, 3)		1392 (3, 1)		74	b_2	1330 (7, 1)	
A_H (40), E_H (10), A_C (40), DE_C (10)	70	b_2	1421 (7, 1)		1433 (20, 5)		75	a_1	1348 (23, 0)	1347
A_H (10), E_H (20), A_C (20), DE_C (45)	71	a_1	1452 (1, 38)	1467	1446 (19, 37)		76	a_1	1375 (0, 5)	
A_H (30), E_H (20), A_C (15), DE_C (30)	72	b_2	1456 (1, 1)				77	b_2	1394 (1, 0)	
E_H (10), A_C (20), DE_C (55)	73	b_2	1466 (4, 4)		1463 (3, 3)		78	a_1	1397 (4, 6)	1405
E_H (15), A_C (30), DE_C (45)	74	a_1	1501 (1, 17)		1488 (34, 6)		79	b_2	1408 (3, 0)	
A_H (30), A_C (60),	75	a_1	1509 (2, 16)		1513 (12, 8)	1525	80	b_2	1410 (4, 3)	
A_H (20), A_C (70), DE_C (5)	76	b_2	1546 (2, 30)		1556 (5, 37)		81	b_2	1439 (7, 3)	
E_H (30), A_C (5), DE_C (65)	77	a_1	1557 (8, 5)	1576	1533 (8, 14)	1569	82	a_1	1462 (1, 34)	1475
E_H (20), A_C (5), DE_C (70)	78	b_2	1577 (8, 13)		1534 (1, 0)		83	b_2	1463 (1, 1)	
A_H (20), A_C (60), DE_C (20)	79	b_2	1586 (12, 23)		1590 (24, 42)		84	b_2	1470 (0, 1)	
A_H (35), A_C (60),	80	a_1	1588 (11, 13)	1594	1593 (20, 11)	1588	85	b_2	1486 (1, 1)	
							86	a_1	1486 (2, 1)	
							87	b_2	1487 (4, 1)	
							88	a_1	1502 (2, 7)	
							89	a_1	1509 (2, 14)	1523
							90	a_1	1541 (5, 7)	1576
							91	b_2	1546 (3, 26)	
							92	b_2	1583 (19, 26)	
							93	a_1	1587 (13, 10)	1597
							94	b_2	1593 (0, 0)	

[a] Potential energy distribution of normal mode of vibration, see text for details. [b] Mode number and symmetry for $ppb^{\bullet-}$ and $ppbCl_2^{-}$. [c] Relative intensities for bands IR and Raman, respectively, normalized such that the most intense band in the reported spectral region is 100. [d] Mode number and symmetry (assuming C_{2v}) for $ppbMe_2^{-}$.

complex.[26] However, the binuclear copper(I) complexes were readily reduced to give a species $[(PPh_3)_2Cu(I)(\mu\text{-}ppb)^{\bullet-}Cu(I)(PPh_3)_2]^+$. There was no evidence of dechelation of the copper ion which has been observed in other related complexes.[27] Reduction of $[(PPh_3)_2Cu(I)(\mu\text{-}ppb)Cu(I)(PPh_3)_2]^{2+}$ resulted in a smooth series of spectral changes (Figure 7) with well-defined isobestic points. The spectra of the reduced copper complexes are similar to each other showing a reduction in the intensity of the MLCT band, with new features growing in to the red, of weak intensity, and blue, of strong intensity (Table 4).

Vibrational Spectral Data. Electrochemical reduction of $[(PPh_3)_2Cu(I)(\mu\text{-}ppb)Cu(I)(PPh_3)_2]^{2+}$ results in dramatic changes to the resonance Raman spectra at a series of excitation wavelengths (457.9, 488.0, and 514.5 nm). This is exemplified by data taken with 514.5 nm excitation (Figure 8): parent species features at 1523, 1500, and 1372 cm^{-1} disappear with application of a reducing potential; concomitant with this behavior a new series of intense bands grow in. The complete absence of these parent species bands indicates that the spectrum observed after reduction has no residual parent species signatures in it. All of the bands observed are assigned to $[(PPh_3)_2Cu(I)(\mu\text{-}ppb)^{\bullet-}Cu(I)(PPh_3)_2]^+$ and attributed to the $ppb^{\bullet-}$ moiety. The resonance Raman spectrum of $[(PPh_3)_2Cu(I)(\mu\text{-}ppbCl_2)Cu(I)(PPh_3)_2]^{2+}$ ($\lambda_{exc} = 457.9$ nm, Figure 8) is also dramatically altered by reduction. Parent species bands at 1365, 1261, and 1100 cm^{-1} are completely bleached upon reduction. Similar behavior is observed for the reduction of $[(PPh_3)_2Cu(I)(\mu\text{-}ppbMe_2)Cu(I)(PPh_3)_2]^{2+}$ with the complete bleaching of parent species bands at 1540, 1454, 1432, 1370, and 1266 cm^{-1}.

(26) Flood, A. H. Ph.D. Thesis, University of Otago, Dunedin, New Zealand, 2001.
(27) Page, S. E.; Gordon, K. C.; Burrell, A. K. *Inorg. Chem.* **1998**, *37*, 4452.

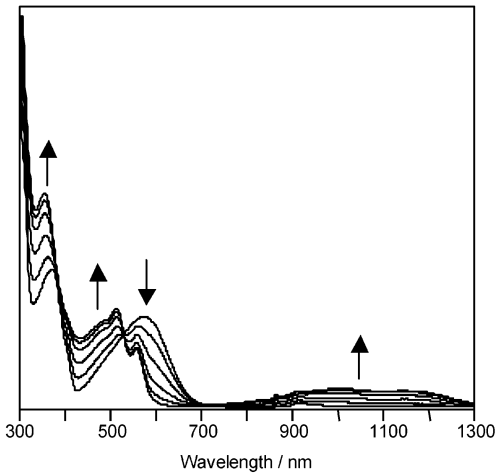

Figure 7. Electronic absorption spectra of $[(PPh_3)_2Cu(\mu\text{-ppb})Cu(PPH_3)_2]^{2+}$ as a function of reducing potential. Absorption dimension is arbitrary. Arrows indicate progressive change in absorbance as the reduction potential becomes more negative (1 mM dichloromethane solution; 0.1 M TBAP supporting electrolyte; applied potential ranged from 0 to 1.0 V; 300−1300 nm region).

A comparison of the calculated Raman spectra of the $ppb^{\bullet-}$-type species with the resonance Raman spectra of the $[(PPh_3)_2Cu(I)(\mu\text{-ppb})^{\bullet-}Cu(I)(PPh_3)_2]^{+}$-type reduced complexes is complicated by the strong modulation of scattering amplitude through the resonance Raman effect.[22,24] The calculated frequencies are useful but the calculated intensities cannot be directly compared to the resonance Raman spectra. Generally, however, within the resonance Raman effect, A-term scattering is dominant and this enhances only totally symmetric modes.[22,28] Hence, in Table 5 the experimentally observed bands are assigned to a_1 modes from the calculated data. A further complication arises because the radical anion data that are experimentally obtained are from a reduced metal complex. Metal moieties can affect the wavenumber of polypyridine vibrations,[29,30] although these are generally modest shifts.

The resonance Raman spectra of the radical anion species show some similarities. In the 1650 to 1550 cm^{-1} region all 3 reduced complexes have a pair of bands lying at 1597−1588 cm^{-1} and 1576−1569 cm^{-1}, which, although very much more intense than the parent complex spectra, are nonetheless at approximately the same frequency as the unreduced species. For $[(PPh_3)_2Cu(I)(\mu\text{-ppb})^{\bullet-}Cu(I)(PPh_3)_2]^{+}$ and $[(PPh_3)_2Cu(I)(\mu\text{-ppbCl}_2)^{\bullet-}Cu(I)(PPh_3)_2]^{+}$ these bands correspond to modes 80 and 77 (Figure 4, Table 5) which are AC and DE in character, respectively. The small frequency shifts upon reduction are consistent with the modest structural changes predicted for the radical anion species. Mode 80 primarily involves stretching of r_2 and r_5 which are unaffected by reduction, and mode 77 is an r_{12}, r_{15} stretch; only r_{15} is altered by reduction.

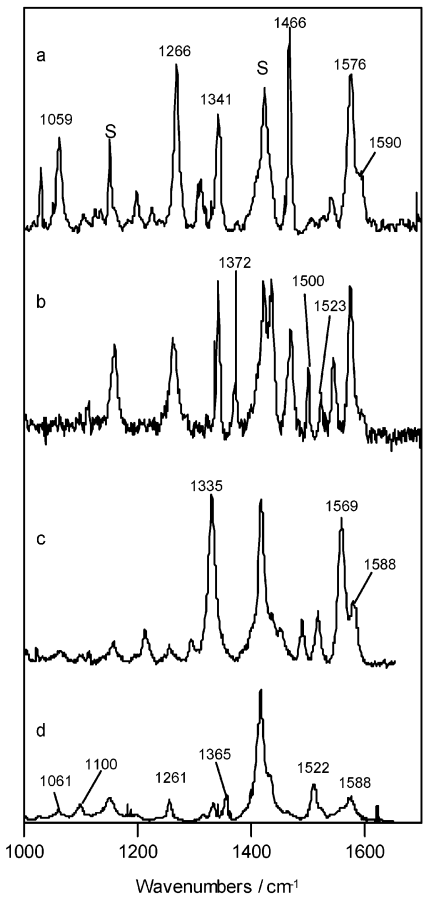

Figure 8. Trace a: Resonance Raman spectrum (λ_{exc} = 514.5 nm) of $[(PPh_3)_2Cu(\mu\text{-ppb})Cu(PPh_3)_2]^{+}$ (3 mM CH_2Cl_2 solution, 0.1 M TBAP electrolyte). Trace b: Resonance Raman spectrum (λ_{exc} = 514.5 nm) of $[(PPh_3)_2Cu(\mu\text{-ppb})Cu(PPh_3)_2]^{2+}$ (3 mM CH_2Cl_2 solution, 0.1 M TBAP electrolyte). Trace c: Resonance Raman spectrum (λ_{exc} = 457.9 nm) of $[(PPh_3)_2Cu(\mu\text{-ppbCl}_2)Cu(PPh_3)_2]^{+}$ (3 mM CH_2Cl_2 solution, 0.1 M TBAP electrolyte). Trace d: Resonance Raman spectrum (λ_{exc} = 457.9 nm) of $[(PPh_3)_2Cu(\mu\text{-ppbCl}_2)Cu(PPh_3)_2]^{2+}$ (3 mM CH_2Cl_2 solution, 0.1 M TBAP electrolyte).

The observation of other different spectral features across the series of reduced complexes is consistent with the calculated structural data, for which the reduction of the ligand results in small bonding changes across the entire structure. These changes range from r_1, r_6 on the ABC rings through to r_{10}, r_{11}, r_{14}, and r_{15} on the DE rings—i.e., the strucutural distortions are not localized to a particular section of the ligand, as is the case in the related dppz ligand.[11]

Conclusions

This study presents structural and spectroscopic data on ppb and its radical anion. The following conclusions may be drawn from this study. (1) The vibrational spectra of ppb and its analogues may be analyzed using ab initio calculations. These calculations, in concert with isotopomer studies, reveal that many of the normal modes of vibration for ppb are localized on selected sections of the structure. (2) Resonance Raman spectroscopy may be used to show that the electronic absorption spectra of $[(PPh_3)_2Cu(\mu\text{-ppbX}_2)Cu(PPh_3)_2]^{2+}$ (where X = H, Cl, CH_3) contain two chromophores that are MLCT in nature, but terminate on

(28) Czernuszewicz, R. S.; Spiro, T. G. In *Inorganic Electronic Structure and Spectroscopy, Volume I, Methodology*; Solomon, E. I., Lever, A. B. P., Eds.; J. Wiley and Sons Inc.: New York, 1999; Chapter 7.
(29) Thornton, D. A.; Watkin, G. M. *J. Coord. Chem.* **1992**, *25*, 299.
(30) Campos-Vallette, M. M.; Clavijo, R. E.; Mendizabel, F.; Zamudio, W.; Baraona, R.; Diaz, G. *Vib. Spectrosc.* **1996**, *12*, 37.

structurally different MOs (ABC and DE-ring based MOs). (3) The structure of the radical anion species may be calculated and compared to experimental data using resonance Raman spectroelectrochemistry of binuclear copper(I) complexes. These show that a number of bands are very similar in frequency across the series, as these represent modes in which the dominant bond length distortions for the normal modes are unaffected by reduction. (4) The calculated structure for the radical anion is very similar to that of the neutral ligand—this suggests why MLCT excited states from ppb are very long-lived. It may be possible to rationally design long-lived MLCT excited states utilizing ab intio calculations.

Experimental Section

Dipyrido[2,3-a:3′,2′-c]phenazine (ppb), dipyrido[2,3-a:3′,2′-c]-6,7-dichlorophenazine (ppbCl$_2$), dipyrido[2,3-a:3′,2′-c]-6,7-dimethylphenazine, (ppbMe$_2$). A typical preparation is as follows. Methanol solutions of equimolar quantities of the appropriate diamino- compound and 4,7-phenanthrolin-5,6-dione (0.760 g, 2.77 mmol) were heated under reflux for 40 min. The solution was cooled to 4 °C, and distilled water (50 mL) was added at which time the product precipitated and was collected by filtration.

Dipyrido[2,3-a:3′,2′-c]phenazine, (ppb). ^{1}H NMR ($CDCl_3$): δ 7.83 (dd, $J = 9$, 6 Hz, 2H); 8.00 (dd, $J = 6$, 3 Hz, 2H); 8.69 (dd, $J = 6$, 3 Hz, 2H); 8.90 (dd, $J = 3$, 3 Hz); 9.30 (d, $J = 6$ Hz, 2H).

Anal. Calcd (0.4 mol MeOH): C, 75.0; H, 3.9; N, 19.0. Found: C, 75.0; H, 4.2; N, 19.4. Yield: 80% (640 mg).

Dipyrido[2,3-a:3′,2′-c]-6,7-dichlorophenazine, (ppbCl$_2$). ^{1}H NMR ($CDCl_3$): δ 7.85 (dd, $J = 8$, 5 Hz, 2H); 8.80 (s, 2H); 8.90 (d, $J = 8$ Hz, 2H); 9.29 (d, $J = 5$ Hz, 2H).

Anal. Calcd (1 mol H_2O): C, 58.5; H, 2.7; N, 15.2. Found: C, 58.7; H, 2.6; N, 15.0. Yield: 82% (820 mg).

Dipyrido[2,3-a:3′,2′-c]-6,7-dimethylphenazine, (ppbMe$_2$). ^{1}H NMR ($CDCl_3$): δ 2.63 (s, 6H); 7.79 (dd, $J = 9$, 3 Hz, 2H); 8.42 (s, 2H); 8.90 (d, $J = 9$ Hz, 2H); 9.28 (d, $J = 3$ Hz, 2H).

Anal. Calcd: C, 77.4; H, 4.5; N, 18.1. Found: C, 77.0; H, 4.5; N, 18.2. Yield: 71% (1.0 g).

Binuclear complexes were prepared by mixing stoichiometric quantities of $[Cu(MeCN)_2(PPh_3)_2](BF_4)$[31] with ligand in chloroform. In a typical preparation 163 mg (2.14×10^{-4} mol) $[Cu(MeCN)_2(PPh_3)_2]$ (BF_4) and 1.07×10^{-4} mol of the appropriate ligand were dissolved in chloroform and stirred for 45 min. The product was collected by evaporation of solvent under vacuum. Crystals of pure product were obtained from chloroform by slow ether diffusion.

[(PPh$_3$)$_2$Cu(μ-ppbCl$_2$)Cu(PPH$_3$)$_2$](BF$_4$)$_2$. Anal. Calcd: C, 63.6; H, 4.0; N, 3.3. Found: C, 63.3; H, 3.9; N, 3.4. Yield: 98% (180 mg).

[(PPh$_3$)$_2$Cu(μ-ppb)Cu(PPh$_3$)$_2$](BF$_4$)$_2$. Anal. Calcd: C, 66.2; H, 4.3; N, 3.4. Found: C, 66.3; H, 4.4; N, 3.1. Yield: 99% (200 mg).

[(PPh$_3$)$_2$Cu(μ-ppbMe$_2$)Cu(PPh$_3$)$_2$](BF$_4$)$_2$. Anal. Calcd: C, 66.6; H, 4.5; N, 3.4. Found: C, 66.6; H, 4.7; N, 3.3. Yield: 98% (200 mg).

Perdeuteration of aromatic species was achieved using a variation on the method of Junk et al.[32] The synthesis of ppb and its isotopomers was developed from literature methods.[33] Selectively deuterated compounds were obtained from the Schiff base reactions of perdeuterated and nondeuterated reactants. For perdeuterated materials the ^{1}H NMR spectra show only singlets, indicating a high level of incorporation of D into the samples. For selectively deuterated samples, such as d_4-ppb, the ^{1}H NMR show only signals from the undeuterated sites, also indicating a high level of D incorporation.

***d*$_4$-1,2-Phenylenediamine.** Yield: 53%. ^{2}H NMR (DMSO) $\delta =$ 6.65(s, 2d) and 6.53(s, 2d). MS (EI) m/z 112 (M^+). Found: C, 64.31; H, 7.21; N, 24.85%. Calcd for $C_6H_4d_4N_2$: C, 64.28; H, 7.19; N, 25.00%.

***d*$_4$-ppb.** Yield: 77% (160 mg). ^{1}H NMR ($CDCl_3$) δ 7.83(d, $J =$ 6 Hz, 2H), 8.92(dd, $J = 6$, 3 Hz, 2H), and 9.31(dd, $J_1 = 6$, 3 Hz, 2H). ^{2}H NMR (DMSO) $\delta = 8.71$(s, 2d) and 8.03(s, 2d).

***d*$_{10}$-ppb.** Yield: 60% (140 mg). ^{2}H NMR (DMSO) δ 9.33(s, 2d), 8.96(s, 2d), 8.73(s, 2d), 8.04(s, 2d), and 7.87(s, 2d).

X-ray Crystallography. Single crystals of complexes $[(PPh_3)_2Cu(\mu\text{-ppbCl}_2)Cu(PPH_3)_2](BF4)_2 \cdot 4H_2O \cdot CH_2Cl_2$ were grown by slow diffusion of diethyl ether into a dichloromethane solution. Suitable crystals were mounted on glass fibers with silicone grease and placed in the cold dinitrogen stream of a Bruker SMART CCD with graphite-monochromated Mo Kα radiation at 90(2) K. Final cell parameters were obtained from a least-squares analysis of reflections with $I > 10\sigma(I)$. Data collection, reduction, solution, and refinement were performed as previously described.[34−36]

Spectral Measurements. ^{1}H and ^{2}H NMR spectra were recorded on a Varian UNITY Inova-300 2-Channel FT 300 MHz or a Varian UNITY Inova-500 2-Channel FT 500 MHz spectrometer. The chemical shift values reported were calibrated with residual solvent signals.

FTIR spectra were collected using a Perkin-Elmer Spectrum BX FTIR system on sample solutions ($CDCl_3$) contained in a transmission cell (0.5-mm path length) with CaF_2 windows.

FT-Raman spectra were collected on powder samples using a Bruker IFS-55 interferometer with an FRA/106 S attachment. The excitation source was an Nd:YAG laser with an excitation wavelength of 1064 nm. A InGaAs diode (D424) operating at room temperature was used to detect Raman photons. All spectra were taken with a laser power of 80 mW at the sample and a resolution of 4 cm^{-1}. Spectra were obtained using 64−256 scans.

A Perkin-Elmer Lamda-19 spectrophotometer was used for collection of electronic absorption spectra. This was calibrated with a Ho_2O_3 filter and spectra were run with a 2-nm resolution.

For electrochemical and spectroscopic measurements, solvents of spectroscopic grade were used. The supporting electrolytes used in the electrochemical measurements were tetrabutylammonium perchlorate (TBAP) and tetrabutylammonium hexafluorophosphate (TBAH). These were purified by repeated recrystallizations from ether/water for TBAP or ethyl acetate/ether for TBAH.[37]

Cyclic voltammograms (CVs) were obtained from argon-purged degassed solutions of compound (ca. 1 mM) with 0.1 M concentration of TBAP or TBAH present. The electrochemical cell consisted of a 1.6- mm diameter platinum working electrode embedded in a Kel-F cylinder with a platinum auxiliary electrode and a saturated potassium chloride calomel reference electrode. The CV was

(31) Yam, V. W.-W.; Lo, K. K.-W. *J. Chem. Soc., Dalton Trans.* **1995**, 499.
(32) Junk, T.; Catallo, W. J.; Elguero, J. *Tetrahedron Lett.* **1997**, *38*, 6309.
(33) (a) Dickeson, J. E.; Summers, L. A. *Aust. J. Chem.* **1970**, *23*, 1023. (b) Gillard, R. D.; Hill, R. E. E.; Maskill, R. *J. Chem. Soc. A* **1970**, 1447.
(34) Waterland, M. R.; Simpson, T. J.; Gordon, K. C.; Burrell, A. K. *J. Chem. Soc., Dalton Trans.* **1998**, 185.
(35) Sheldrick, G. M. SHELXL 95, Institut für Anorganische Chemie der Universität Göttingen, 1993.
(36) Johnson, C. K. ORTEP II, Report ORNL-5138, Oak Ridge National Laboratory: Oak Ridge, TN, 1976.
(37) House, H. O.; Feng, E.; Peet, N. P. *J. Org. Chem.* **1971**, *36*, 2371.

calibrated against ferrocene/ferrocenium couple. The potential of the cell was controlled by an EG&G PAR 273A potentiostat with model 270 software.

Resonance Raman scattering was generated using a Melles Griot OmNichrome model 543-MAP argon ion laser. For a 457.9-nm laser a Kaiser Optical Systems holographic laser bypass filter was used. The sample was held in a spinning NMR tube or an optically transparent thin-layer electrode (OTTLE) cell, and the scattering was collected in a 135° backscattering geometry. The irradiated volume was imaged into a Spex 750M spectrograph using a two-lens arrangement. The spectrograph was equipped with an 1800 g/mm holographic grating which provided a dispersion of 0.73 nm/mm. The Raman photons were detected using a Princeton Instruments liquid nitrogen cooled 1152-EUV charge-coupled detector controlled by a Princeton Instruments ST-130 controller. CSMA v2.4 software (Princeton Instruments) was used to control the CCD, and spectra were analyzed using GRAMS/32 (Galactic Industries Corp.) software. Spectral windows were approximately 18 nm wide and were calibrated using emission lines from a neon or krypton lamp. The calibrations were checked by measuring the Raman band frequencies for known solvents.[38] Rayleigh and Mie scattering from the sample was attenuated using a Notch filter (Kaiser Optical Systems Inc.) of appropriate wavelength. A polarization scrambler was placed in front of the spectrograph entrance slit. A 150-μm slit width was used on the spectrograph, and this gave resolution of ca. 6 cm^{-1} with 457.9 nm excitation.

The electronic absorption spectra of reduced species were measured using an OTTLE cell with a platinum grid as the working electrode.[34] For Raman spectra of the reduced species, a similar cell was employed. Initial measurements found that the signal-to-noise of the Raman spectra were reduced because of reflection off the platinum grid. This problem was alleviated by removing a portion of the center of the grid (ca. 2 mm $\times$ 4 mm) and aligning the laser to irradiate the solution in that region. For electronic absorption spectroelectrochemistry spectra were acquired at a series of applied potentials stepping through the oxidation or reduction of interest. For Raman studies the applied potential was set beyond the $E^{0/}$ value of the electrochemical process, and data were collected after sufficient time that the probed volume contained only the reduced or oxidized product.

Computational Studies

The geometry optimizations, vibrational frequencies, and their IR and Raman intensities were calculated using DFT calculations (B3LYP functional, 6-31G(d) basis set). These were implemented with the Gaussian 98[39] and 94[40] program packages. The visualization of the MOs and vibrational modes was provided by the Molden package.[41]

Acknowledgment. Support from the The MacDiarmid Institute for Advanced Materials and Nanotechnology and the New Economy Research Fund is gratefully acknowledged. S.L.H. thanks the Foundation for Research Science and Technology for the award of a PhD scholarship.

Supporting Information Available: Crystallographic information (cif) and vibrational data (pdf) for the subject compounds. This material is available free of charge via the Internet at http://pubs.acs.org.

IC030225L

(38) (a) McCreery, R. L. *Raman Spectroscopy for Chemical Analysis*; Wiley Chemical Analysis Series, Vol. 157; Winefordner, J., Ed.; John Wiley: New York, 2000. (b) The ASTM subcommitte on Raman spectroscopy has adopted eight materials as Raman shift standards (ASTM E 1840). The band wavenumbers for these standards are available at http://chemistry.ohio-state.edu/~rmccreer/shift.html.

(39) Frisch, M. J.; Trucks, G. W.; Schlegel, H. B.; Scuseria, G. E.; Robb, M. A.; Cheeseman, J. R.;. Zakrzewski, V. G; Montgomery, J. A., Jr.; Stratmann, R. E.; Burant, J. C.; Dapprich, S.; Millam, J. M.; Daniels, A. D.; Kudin, K. N.; Strain, M. C.; Farkas, O.; Tomasi, J.; Barone, V.; Cossi, M.; Cammi, R.; Mennucci, B.; Pomelli, C.; Adamo, C.; Clifford, S.; Ochterski, J.; Petersson, G. A.; Ayala, P. Y.; Cui, Q.; Morokuma, K.; Malick, D. K.; Rabuck, A. D.; Raghavachari, K.; Foresman, J. B.; Cioslowski, J.; Ortiz, J. V.; Baboul, A. G.; Stefanov, B. B.; Liu, G.; Liashenko, A.; Piskorz, P.; Komaromi, I.; Gomperts, R.; Martin, R. L.; Fox, D. J.; Keith, T.; Al-Laham, M. A.; Peng, C. Y.; Nanayakkara, A.; Gonzalez, C.; Challacombe, M.; Gill, P. M. W.; Johnson, B.; Chen, W.; Wong, M. W.; Andres, J. L.; Head-Gordon, M.; Replogle, E. S.; Pople, J. A. *Gaussian 98, Revision A.7*; Gaussian, Inc.: Pittsburgh, PA, 1998.

(40) Frisch, M. J.; Trucks, G. W.; Schlegel, H. B.; Gill, P. M. W.; Johnson, B. G.; Robb, M. A.; Cheeseman, J. R.; Keith, T.; Petersson, G. A.; Montgomery, J. A.; Raghavachari, K.; Al-Laham, M. A.; Zakrzewski, V. G.; Ortiz, J. V.; Foresman, J. B.; Cioslowski, J.; Stefanov, B. B.; Nanayakkara, A.; Challacombe, M.; Peng, C. Y.; Ayala, P. Y.; Chen, W.; Wong, M. W.; Andres, J. L.; Replogle, E. S.; Gomperts, R.; Martin, R. L.; Fox, D. J.; Binkley, J. S.; Defrees, D. J.; Baker, J.; Stewart, J. P.; Head-Gordon, M.; Gonzalez, C.; Pople, J. A. *Gaussian 94, Revision D.4*; Gaussian, Inc.: Pittsburgh, PA, 1995.

(41) Schaftenaar, G.; Noordik, J. H. *J. Comput.-Aided Mol. Des.* **2000**, *14*, 123.